

# AIForge-Doc: A Benchmark for Detecting AI-Forged Tampering in Financial and Form Documents

Jiaqi Wu\*, Yuchen Zhou\*, Muduo Xu, Zisheng Liang, Simiao Ren†, Jiayu Xue, Meige Yang, Siying Chen, Jingheng Huan

\*Equal contribution †Corresponding author

Duke University: {jw933, yz946, zisheng.liang, siying.chen, jingheng.huan}@duke.edu

New York University: mx2336@nyu.edu University of North Carolina: xuejiayu@unc.edu

Scam.ai: benren@scam.ai University of Southern California: maggiaya@usc.edu

## Abstract

We present **AIForge-Doc**, the first dedicated benchmark targeting *exclusively* diffusion-model-based inpainting in financial and form documents with pixel-level annotation. Existing document forgery datasets rely on traditional digital editing tools (e.g., Adobe Photoshop, GIMP), creating a critical gap: state-of-the-art detectors are *blind* to the rapidly growing threat of AI-forged document fraud. AIForge-Doc addresses this gap by systematically forging numeric fields in real-world receipt and form images using two AI inpainting APIs—GEMINI 2.5 FLASH IMAGE and IDEOGRAM V2 EDIT—yielding **4,061** forged images from four public document datasets (CORD, WildReceipt, SROIE, XFUND) across nine languages, annotated with pixel-precise tampered-region masks in DocTamper-compatible format. We benchmark three representative detectors—TruFor [7], DocTamper [22], and a zero-shot GPT-4o judge—and find that all existing methods degrade substantially: TruFor achieves  $AUC=0.751$  (zero-shot, out-of-distribution) vs.  $AUC=0.96$  on NIST16; DocTamper achieves  $AUC=0.563$  vs.  $AUC=0.98$  in-distribution, with pixel-level IoU=0.020; GPT-4o achieves only **0.509**—essentially at chance—confirming that AI-forged values are indistinguishable to automated detectors and VLMs. These results demonstrate that AIForge-Doc represents a qualitatively new and unsolved challenge for document forensics.

## 1 Introduction

Document fraud is an escalating global problem. Digital document forgeries increased **244%** year-over-year in 2024, and for the first time digital forgeries (57%) surpassed physical counterfeits as the dominant fraud method [4]—a 1,600% increase since 2021. A deepfake or AI-manipulated document attempt occurred every five

minutes during 2024, with generative AI tools cited as the primary enabler. Historically, document forgery required expert knowledge of image editing software, leaving characteristic traces—compression artifacts, cloning patterns, statistical anomalies in noise residuals—that computational forensic methods can reliably detect.

The arrival of generative AI has fundamentally changed this threat landscape. State-of-the-art diffusion-model-based inpainting APIs (e.g., Gemini 2.5 Flash Image, Ideogram v2 Edit) can now convincingly replace a specific word or number in a document photograph while seamlessly blending with the surrounding font, texture, and background—all in under one second and at approximately \$0.01 per edit. Unlike Photoshop-based edits, AI-forged regions exhibit no obvious compression seams or cloning signatures; instead, the generator synthesizes plausible-looking pixels that are statistically consistent with the original, making detection fundamentally harder.

**The dataset gap.** Despite the urgency of this threat, no public benchmark exists for evaluating detectors against AI-forged document tampering. The leading document-specific forgery datasets—DocTamper [22] (170k images), RTM [15] (9k images), and the ICDAR 2023 TII benchmark [16] (11k images)—all use traditional copy-move, splicing, or typesetting manipulation. Even the most recent OSTF benchmark [23], while including diffusion-based methods, focuses on scene-text images (storefronts, signs) rather than financial or form documents, and uses bounding-box rather than pixel-level mask annotation. Crucially, even if a detector were trained on OSTF-style scene-text AI forgeries, there is no guarantee it would generalize to the different visual domain and targeted numeric manipulation of financial receipts and form documents—a gap our empirical evaluation (§6) confirms. General-purpose image forgery datasets (COVERAGE [34], Columbia [9], CASIA [3], NIST16 [6]) are similarly free of AI-generated

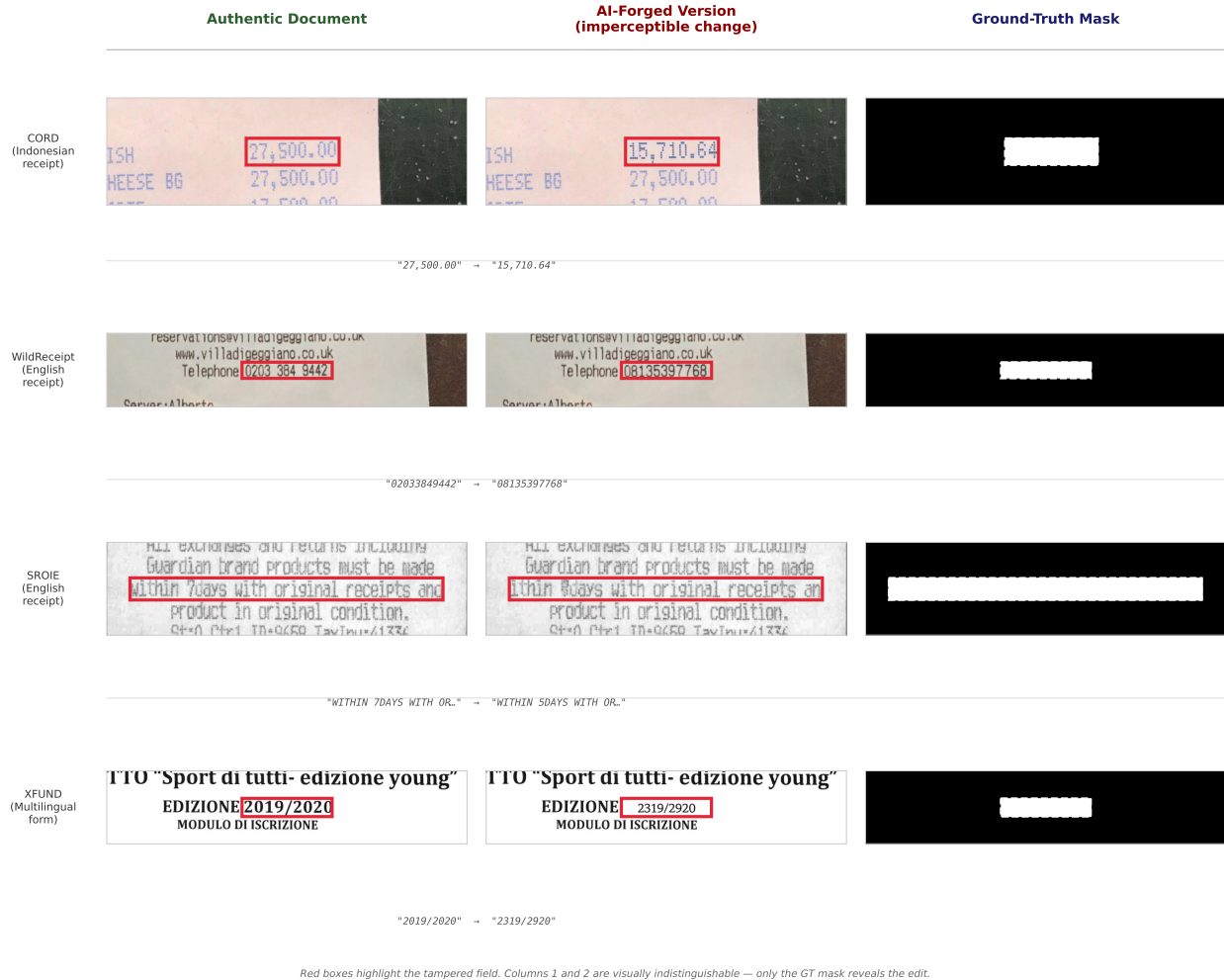


Figure 1: **AIForge-Doc: AI-inpainted document forgeries pass visual inspection and are difficult to distinguish from authentic documents.** Each row: authentic document with target field highlighted (left), AI-forged version (center), pixel-precise ground-truth mask (right). From top: CORD receipt (Ideogram v2 Edit), WildReceipt (Gemini 2.5 Flash Image), SROIE receipt (Gemini), XFUND multilingual form (Ideogram v2 Edit). The tampered region—a single numeric field—comprises a median of 0.9% of image pixels, yet contains the forensically critical edit.

content. Detectors trained on these corpora are therefore evaluated exclusively on the distribution they were designed for, with no guarantee of robustness to the qualitatively different artifacts produced by neural inpainting in financial documents.

**Our contribution.** We introduce **AIForge-Doc**, the first benchmark *targeting exclusively* diffusion-model-based inpainting in financial and form documents with pixel-level annotation, with three core contributions:

1. **A novel dataset of AI-forged document images.** We systematically tamper with numeric fields in 4,061 source images from four public datasets using two AI inpainting APIs (Gemini 2.5 Flash Image and Ideogram v2 Edit), selected from seven evaluated systems (five re-

jected for garbled text output or insufficient resolution), yielding 4,061 forged images with pixel-precise ground-truth masks in an 80/20 train/test split. Field types vary by dataset: financial amounts (CORD), telephone and address numerics (WildReceipt), text-embedded numbers (SROIE), and form answer fields (XFUND). The training partition (3,249 images) is intended as a resource for the community to develop and train future detectors specifically targeting AI-inpainting artifacts.

2. **A reproducible generation pipeline.** We release a fully automated open-source pipeline that ingests raw source documents, selects high-priority numeric fields, generates plausible alternative values, runs context-window inpainting via local or API-accessed models, and packages results in DocTamper-compatible format.

3. **A baseline evaluation revealing a critical detection gap.** We benchmark TruFor [7], DocTammer [22], and GPT-4o zero-shot on AIForge-Doc and find substantial degradation: TruFor achieves AUC=0.751 on AIForge-Doc (zero-shot) vs. 0.96 on NIST16 (per original authors); DocTammer achieves AUC=0.563 on AIForge-Doc vs. 0.98 on its own in-distribution test set, with IoU falling from 0.71 to 0.020; GPT-4o achieves only 0.509—essentially random. This establishes AI-forged document tampering as an open and important research problem.

**Scope and limitations.** AIForge-Doc focuses on *localized numeric field forgery* in receipts and form documents—the highest-risk scenario for financial fraud. We do not cover wholesale document synthesis (e.g., GAN-generated identity documents from scratch), signature forgery, or LLM-generated textual fraud, which we consider complementary and leave for future work.

## 2 Related Work

### 2.1 Document Forgery Datasets

**Document text tampering datasets.** DocTammer [22] (CVPR 2023) is the largest prior work: 170,000 document images (contracts, invoices, receipts) with character- and word-level text substitution, insertion, and deletion—all traditional typesetting edits with no AI-generated content. RTM [15] (*Pattern Recognition* 2024) provides 9,000 images including 6,000 manually tampered by professional editors, revealing that detectors trained on synthetic forgeries fail on human-crafted real-world ones. The ICDAR 2023 TII dataset [16] adds 11,385 images across classification and localization tracks.

**OSTF and AI-inpainting benchmarks.** OSTF [23] (AAAI 2025) is the closest predecessor, assembling 4,418 images by replacing text regions with outputs from eight methods (four diffusion-based, four conventional) in natural scene-text photographs (storefronts, signs, menus). AIForge-Doc differs from OSTF along four axes. *Document type:* OSTF targets open-domain scene-text; AIForge-Doc exclusively targets financial receipts and structured forms, where numeric field tampering carries direct fraud consequences—a forged total on a receipt constitutes financial fraud in a way that a wrong number on a storefront sign does not. *Threat model:* OSTF benchmarks a broad spectrum of manipulation methods (4 diffusion + 4 conventional); AIForge-Doc isolates the specific threat posed by consumer-accessible diffusion APIs (Gemini 2.5 Flash Image, Ideogram v2 Edit), where a non-expert can

forge a document in under one second for \$0.01. *Annotation format:* OSTF uses word-level polygon masks and reports bounding-box AP metrics; AIForge-Doc provides full-image binary masks in DocTammer-compatible format, enabling direct IoU/AUC-based comparison with existing document forensics methods. *Generalization gap:* Most critically, OSTF demonstrates that AI text replacement is detectable when detectors are trained on the appropriate manipulation distribution. AIForge-Doc asks a harder and distinct question: *does knowledge of AI scene-text forgeries transfer to targeted financial document forgery?* Our zero-shot evaluation (Section 6) provides evidence that it does not—TruFor achieves AUC=0.751 and DocTammer AUC=0.563 despite strong performance on their respective training distributions—establishing financial document forgery as an open research problem even given the existence of OSTF-style training data. AIForge-Doc is also publicly released without registration. FGD TD [21] (2025) introduces fine-grained tampering classification over 16,479 images across 12 source datasets. SAGI [5] provides 95,000+ AI-inpainted images across multiple diffusion pipelines; AIForge-Doc complements it by focusing specifically on document content and targeted numeric-field manipulation.

**General image forgery datasets.** Columbia [9], COVERAGE [34], CASIA [3], NIST MFC [6], and FF++ [31] are standard benchmarks for copy-move, splicing, and deepfake detection in natural photographs; none target document images or AI-based inpainting.

### 2.2 Tampering Detection Methods

**General forensic detectors.** ManTraNet [35], CAT-Net [12], PSCC-Net [14], HiFi-Net [8], and IML-ViT [17] represent the range of general-purpose image forgery detectors. Ren et al. [26] demonstrate that state-of-the-art deepfake detectors frequently fail to generalize to real-world conditions outside their training distribution, a finding directly echoed in our zero-shot evaluation on AI-forged document content. TruFor [7] (CVPR 2023) is the current state of the art, combining a transformer backbone with NoisePrint++, a learnable camera-model fingerprint, to achieve strong generalization across manipulation types; we use it as our primary baseline.

**Document-specific detectors.** DocTammer’s detector [22] is the only published method trained specifically on document forgeries. It incorporates document-specific priors via frequency-domain auxiliary losses, achieving substantial gains over general detectors on its own test set. We evaluate it zero-shot on AIForge-Doc to measure the generalization gap to AI-forged content.

**LLM/VLM as forensic judges.** [27] benchmark multi-modal LLMs (including GPT-4o and Gemini) against traditional deepfake detectors. [13] extend this to fraudulent document detection via prompt optimization—the closest precedent to our GPT-4o baseline. We include GPT-4o zero-shot to measure what world-knowledge reasoning can achieve without labeled training data.

### 2.3 AI Inpainting and Its Forensic Signatures

Diffusion-model-based inpainting [1, 30] achieves photorealistic local edits by conditioning denoising on a masked region. [2] and [29] study detection of diffusion-generated images at the full-image level. Ren et al. [28] provide a comprehensive zero-shot benchmark of 16 open-source AI-generated image detectors across 12 datasets, finding no universal winner—a breadth finding complementary to our targeted in-document localization study. Detection of *localized* diffusion inpainting within otherwise authentic documents is far less studied and represents the core challenge in AIForge-Doc.

## 3 Dataset Construction

### 3.1 Source Document Datasets

AIForge-Doc is built on top of four publicly available document datasets spanning receipts and forms in multiple languages (Table 1).

**CORD v2 [20].** The Consolidated Receipt Dataset contains 1,000 scanned receipt images in Indonesian with comprehensive key-value annotations for  $\sim 30$  field types including item names, unit prices, subtotals, and total prices. We use the full 1,000-image split, prioritizing `menu.price`, `total.totalprice`, and `sub.total.subtotalprice` fields.

**WildReceipt [33].** An open-domain English receipt dataset with approximately 1,740 images collected from diverse scanners and mobile cameras, annotated with 25 key-value field types. We use 1,696 images from the released split. Financial amount fields are labeled with IDs 13–14 (product price), 19–20 (tax), and 23–24 (total).

**SROIE [10].** The ICDAR 2019 Scanned Receipt OCR and Information Extraction dataset contains 626 training and 347 test receipt images with four key fields: *company*, *date*, *address*, and *total*. We target numeric fields, prioritizing *total* (financial amount) and *date*; when these are unavailable the field selector falls back to address-embedded numerics and policy-text fields containing numeric values

(e.g., return windows such as “WITHIN 7 DAYS”), using 946 images.

**XFUND [36].** A multilingual form understanding dataset in seven non-English languages (ZH, JA, ES, FR, IT, DE, PT) with key-value annotations. We target numeric answer entities, contributing 419 images. XFUND forms are high-resolution A4 scans (up to  $4961 \times 7016$  px at 600 dpi).

### 3.2 Field Selection and Value Mutation

**Field prioritization.** For each source image, we select the single highest-priority numeric field according to: (1) financial amount, (2) date, (3) document ID/number, (4) quantity, (5) other numeric. This focuses the dataset on the highest-risk forgery scenarios for financial fraud.

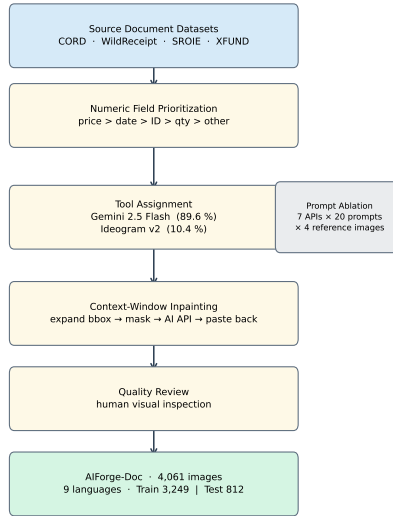
**Value mutation.** We generate plausible alternative values that look realistic but differ from the original:

- **Monetary fields:** Multiply by a random scale factor drawn from  $\mathcal{U}(1.15, 3.0)$  (scale up) or  $\mathcal{U}(0.20, 0.85)$  (scale down), applied with 50% probability each, producing a roughly symmetric distribution of scaled-up and scaled-down forgeries. The mutation loop retries up to 30 times to find a value with the same character count as the original, minimizing visual discrepancy in fixed-width fonts; if unsuccessful, digit-flipping is used as a fallback (which preserves length by construction).
- **Date fields:** Perturb year by  $\pm 1-5$ , month by  $\pm 1-3$ , or day by  $\pm 3-15$ , with calendar validity enforced.
- **Document IDs:** Flip 1–2 randomly selected digits.
- **Quantities:** Multiply by  $2-5 \times$ .

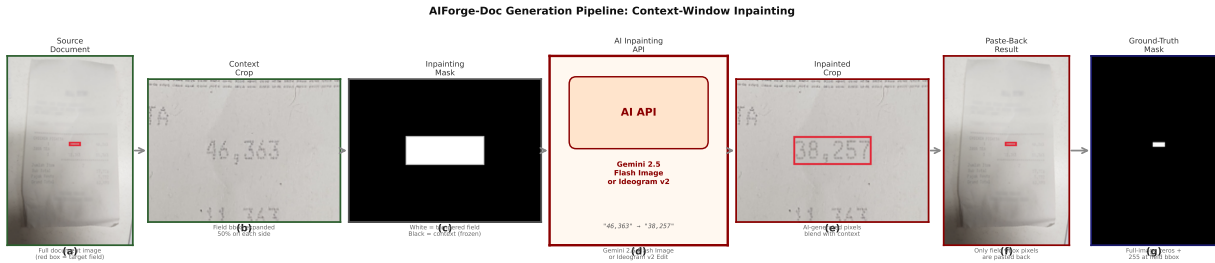
### 3.3 Context-Window Inpainting Technique

A critical design choice is the *context-window* approach illustrated in Fig. 2. Naïvely feeding an entire document image to an inpainting model (a) risks global drift: the model may hallucinate backgrounds or alter surrounding text. Instead, we:

1. Expand the field bounding box by 50% on each side (minimum 150 px padding) to create a *context crop* that includes neighboring characters for font reference.
2. Create a binary mask on the context crop: white (255) over the field, black (0) elsewhere.
3. Run inpainting on the context crop only with a font-preserving prompt (Section 3.3).
4. Paste *only the field region* (original bbox, no padding) from the inpainted context back into the full-resolution source image.



(a) Overall dataset creation workflow.



(b) Per-image context-window inpainting technique (steps a–f).

Figure 2: **AIForge-Doc generation pipeline.** *Top*: the overall dataset creation workflow, from source datasets through field selection and tool assignment (informed by a 320-trial prompt ablation study) to the final DocTamper-compatible dataset. *Bottom*: the per-image context-window inpainting technique—starting from a source document (a), we expand a context crop (b), create a binary inpainting mask (c), feed the crop and mask to the AI API (d), and paste only the field region back into the full image (e) to produce the forged output and pixel-precise ground-truth mask (f).

5. Generate the ground-truth mask as a full-image binary PNG with 255 at the exact field bbox and 0 everywhere else.

This guarantees that (i) the model sees surrounding text for font/color reference, (ii) only pixels within the field bbox are altered in the final image, and (iii) the ground-truth mask is pixel-perfect. The paste-back step (step 4) is the key safeguard: regardless of what the inpainting model does to surrounding pixels in the context crop, only the exact field bbox region is ever written back to the source image, ensuring mask accuracy by construction rather than by relying on the model’s compliance with the prompt. To verify that Gemini’s editing does not affect regions outside the declared bbox, we compared non-bbox pixels between originals and forged images across 200 randomly sampled Gemini outputs and found that the context-

window paste-back step eliminates any out-of-bbox drift by construction—since only the exact field region is pasted from the inpainted context into the full image.

**Inpainting prompt.** All tools receive the following templated prompt:

*“Change only the text in the masked region to read ‘{new\_value}’. Preserve the exact font family, weight, size, letter-spacing, color, and vertical baseline of the surrounding characters on the same line. Do not alter the background texture, borders, lines, or any other element. The edit must be visually indistinguishable from the original document.”*

### 3.4 AI Inpainting Tools

We prototyped seven AI inpainting systems and deployed two for mass generation.

#### Deployed tools (2).

- **Gemini 2.5 Flash Image** (OpenRouter): Google’s multi-modal model with image generation capability, accessed via `google/gemini-2.5-flash-image`. Gemini does not accept a binary mask tensor; instead we draw a 3-pixel bright-green rectangle on the context crop to mark the edit region and reference it in the prompt.
- **Ideogram v2 Edit** (fal.ai): A high-fidelity text-rendering inpainting system [11], particularly suited for typographic content. Accessed via `fal-ai/ideogram/v2/edit`.

**Evaluated but disabled tools (5).** We systematically evaluated five additional inpainting systems through a prompt ablation study (Section 3.7; Fig. 3): for each API-accessible tool, we tested 20 diverse prompt formulations on four reference images across all source datasets (320 trials total).

**FLUX Fill Pro** [1]: generates plausible digit shapes but consistently *wrong values* (e.g., “112,800” or “155,700” instead of target “196,718”), with inconsistent font weight across all 20 prompt variants.

**SD 3.5 Medium** [32]: the worst performer; frequently renders the *prompt text itself* into the image (e.g., “Replace Text,” “Restore Beautifully”) or produces garbled characters and emoji, ignoring the inpainting task entirely regardless of prompt formulation.

**GPT-Image-1** [18]: falls back to DALL-E-2 [24] at  $512 \times 512$  px; occasionally produces correct numerals but with mismatched font size, excessive boldness, and blurry upscaling artifacts that fail human review.

**SD 1.5 Inpainting** [30]:  $512 \times 512$  native resolution produces uniform blurry patches; text is entirely unreadable at document scale.

The remaining tool, **FLUX Fill Dev** [1], requires 24 GB VRAM and was not available for mass generation; it shares the FLUX architecture with Fill Pro and similarly lacks multimodal text understanding.

Across all 320 ablation trials, *zero* outputs from any rejected tool met our quality bar. The failure is architectural: only models with multimodal language understanding (Gemini 2.5 Flash Image, Ideogram v2 Edit) can perform character-accurate text replacement in document images. AIForge-Doc therefore concentrates on these two tools. Pipeline code and ablation results for all seven tools are released for reproducibility.

### 3.5 Engineering Adaptations

Several non-trivial implementation challenges arose during large-scale generation; we document them here for reproducibility.

**Gemini mask encoding.** As noted above, Gemini does not accept a binary mask tensor. To improve text legibility on small fields, we  $2 \times$  upsample the context crop (LANCZOS) before sending to the API and downsample the result before pasting back.

**Ideogram content filtering.** The Ideogram v2 Edit API applies an internal content safety checker that flagged 83 requests ( $\approx 16.6\%$  of Ideogram specs), predominantly from SROIE receipts containing real Malaysian business addresses and registration numbers, and XFUND forms with government document content. Our pipeline distinguishes *content-filter failures* (matched on `content_policy_violation`) from ordinary API errors: content-filtered requests are immediately skipped and logged to `skipped_specs.jsonl`; ordinary errors trigger exponential-backoff retry (3 attempts: 5 s, 10 s, 20 s); budget-exhaustion errors halt generation entirely. All 81 unique skipped Ideogram specs were resubmitted to Gemini and completed successfully, yielding zero net data loss. The 81 rerouted specs are labeled in metadata with `assigned_tool=gemini` and are excluded from the Ideogram subset in per-tool analysis.

**Separator hint in prompt.** Early Ideogram outputs frequently omitted thousand-separator commas (e.g., “75000” instead of “75,000”). We append a separator hint to the prompt: “Use {sep} as the thousands separator,” where {sep} is inferred from the original value.

**Value length matching.** When the mutated value has a different character count from the original, the inpainting model must render more or fewer glyphs into the same bounding box, which degrades quality. As described in Section 3.2, the mutation loop retries up to 30 times to find a length-matched value before falling back to digit-flipping.

### 3.6 Quality Control

Quality control proceeds in three stages applied to all 4,061 generated images:

1. **Automated OCR check (all images).** As a coarse pre-filter, each forged image is validated with `PadleOCR` [19]: we crop the tampered bbox region and verify that the OCR output contains at least one recognized token. Images where the model produced a

blank, smeared, or hallucinated result are flagged and excluded; this step removes obviously broken outputs before human review.

2. **Human review (all images).** Every generated image was reviewed by the authors via side-by-side preview panels (original vs. forged, with the tampered bbox highlighted)—the primary quality gate. Images with blank, garbled, or visually incoherent output are flagged immediately; all 4,061 final images passed this review.
3. **Semantic plausibility check (metadata validation).** We verify that the forged value differs from the original value for every image, filtering any edge cases where the mutation loop produced an identical value.

This three-stage pipeline complements the upstream tool screening (Section 3.4), where 5 of 7 prototyped models were eliminated because they consistently produced garbled or illegible text output—ensuring that AIForge-Doc contains only forgeries at the quality frontier of current AI inpainting capability. A final manual pass over the complete 812-image testing set confirmed legible, realistic-looking text in every case.

### 3.7 Prompt Ablation Study

A natural concern is whether the five rejected tools (Section 3.4) might succeed under different prompt formulations. To address this, we conducted a systematic prompt ablation: for each of the four API-accessible rejected tools (FLUX Fill Pro, GPT-Image-1, SD 3.5 Medium, and SD 1.5 Inpainting), we tested **20 diverse prompts on four reference images**—one from each source dataset (CORD, SROIE, XFUND, WildReceipt)—where Gemini 2.5 Flash Image had already produced high-quality forgeries, yielding  $4 \times 20 \times 4 = 320$  inpainting trials total.

**Prompt diversity.** The 20 prompts span a wide spectrum of strategies: (i) *minimal* (bare target value only), (ii) *imperative* (“Replace masked text with . . .”), (iii) our *production template* used for mass generation, (iv) *character-by-character* spelling of the target value, (v) *chain-of-thought* (analyze surrounding typography, then act), (vi) *role-play* variants (document restoration specialist, Photoshop retoucher, forensic examiner), (vii) *typography expert* (match typeface, kerning, leading, stroke weight), (viii) *negative constraints* (“Do NOT change pixels outside the mask”), and (ix) *verbose exhaustive* (8-point numbered requirements list). The full prompt set is provided in our released code.

**Results.** Figure 3 shows representative outputs. None of the 320 trials produced output meeting our quality bar.

Table 1: Source datasets in AIForge-Doc.

Dataset	Doc Type	Lang	Images	Fields
CORD v2 [20]	Receipt	id	1,000	price, total
WildReceipt [33]	Receipt	en	1,696	tel, addr, price
SROIE [10]	Receipt	en	946	total, date
XFUND [36]	Form	multi	419	answer (num)
<b>Total</b>	—	—	<b>4,061</b>	—

Crucially, *no prompt strategy*—including detailed chain-of-thought reasoning, domain-expert role-play, and verbose multi-constraint specifications—overcame these limitations. The two deployed tools succeed because they possess multimodal language understanding that enables character-accurate text rendering; the rejected tools, as pure image-synthesis diffusion models, lack this capability regardless of prompt engineering.

## 4 Dataset Statistics and Analysis

### 4.1 Scale and Composition

AIForge-Doc contains **4,061** forged images derived from 4,061 source images across four receipt and form datasets (Table 1). Each source image contributes exactly one forged image (single field, single tool), maintaining a clean one-to-one correspondence between authentic and forged examples.

**Field type distribution.** Field selection follows the prioritization scheme in Section 3.2 (financial amount > date > document ID > quantity > other numeric). In practice, the selected field type is determined by each source dataset’s annotation structure, and the distribution reflects their coverage rather than the priority ordering: CORD images predominantly contribute financial amount fields (`menu.price`, `total.total_price`, `sub.total.subtotal_price`), which are richly annotated. WildReceipt has limited financial amount annotations accessible at the field level; the priority scheme therefore falls back to other labeled numeric fields—primarily telephone numbers (`Telephone_key`,  $n=931$ ) and store address numerics (`Store_addr_key`,  $n=457$ )—which are the most abundant numeric annotations in that dataset. SROIE’s available annotations are contact and return-policy text fields containing embedded numeric values (e.g., “WITHIN 7 DAYS WITH RECEIPTS”), along with a subset of date fields. XFUND images contribute numeric `answer` fields from multilingual forms. While the dataset therefore spans a broader range of document numeric fields than pure financial amounts, every selected field is a plausible target for document fraud: forging a business telephone

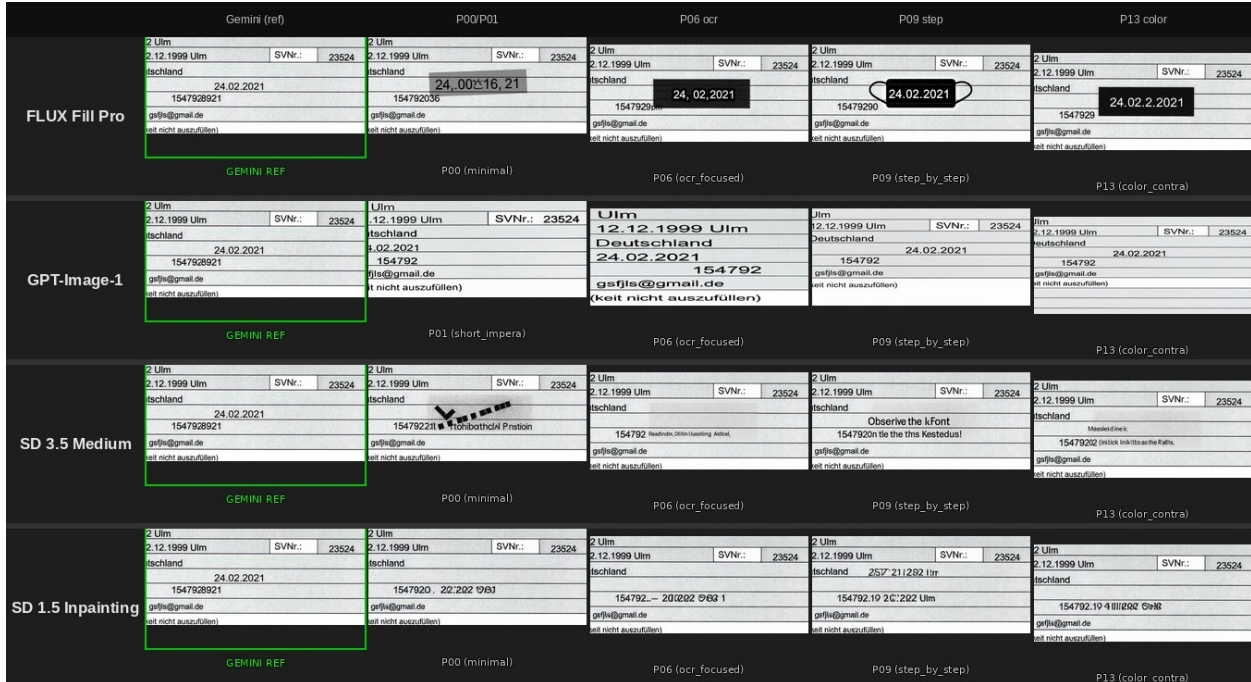


Figure 3: **Prompt ablation: 5 representative outputs per rejected tool on WildReceipt image 00002699 (Prod.item\_key, “HULAHAWAIIANT1”→“HULAHAWAIIANT4”).** Each row shows the Gemini 2.5 Flash reference (green border) alongside outputs from four prompt strategies spanning minimal, OCR-focused, step-by-step, and color-aware prompts. FLUX Fill Pro renders plausible digit shapes but consistently wrong values; GPT-Image-1 produces a black N/A patch or blurry wrong-font text at 512 px; SD 3.5 Medium renders prompt text literally or produces garbled symbols; SD 1.5 Inpainting yields illegible blurred patches. No prompt strategy succeeds for any rejected tool. Full 20-prompt-variant grids are in Figs. 6 to 9 (Appendix B).

number, address code, or policy date can mislead document verification just as a forged total can. The dataset is thus best characterized as an *AI-forged document field* benchmark, with CORD providing the most forensically critical financial amount examples.

**Tool distribution.** Gemini 2.5 Flash Image accounts for 89.6% of forgeries (3,639 images) and Ideogram v2 Edit for 10.4% (422 images). The primary driver of this imbalance is *output quality*: we prioritize dataset quality over tool balance, and Ideogram v2 Edit was restricted to the CORD and WildReceipt subsets where its typographic output consistently met our quality bar. On SROIE and XFUND content, Ideogram’s content safety filter rejected 83 requests ( $\approx 16.6\%$  of its allocated specs, see Section 3.5), and the remaining outputs on those document types showed lower typographic fidelity than Gemini; those specs were therefore rerouted to Gemini. Ideogram’s per-image cost ( $2\times$  Gemini’s) further reinforced the decision to concentrate Gemini usage where Ideogram underperformed. The 20/80 stratified split yields 85 Ideogram and 727 Gemini images in the test set, reflecting this quality-driven composition. This imbalance has forensic

significance: the two tools leave detectably different artifact signatures, and the asymmetric test-set ratio must be accounted for when interpreting per-tool detection results (Section 6).

**Data partitions.** We release a fixed 80/20 partition (3,249 / 812 images), stratified by source dataset and tool. All baseline experiments in Section 6 are zero-shot evaluations on the test partition.

## 4.2 Mask Format

Ground-truth masks follow the DocTamper convention:

- 8-bit grayscale PNG, same resolution as the source image.
- Pixel value 0: authentic region.
- Pixel value 255: tampered region.
- Tampered region = the exact field bounding box (tight, no padding).

Figure 1 (page 1) shows representative authentic/forged image pairs with their ground-truth masks across four source datasets.

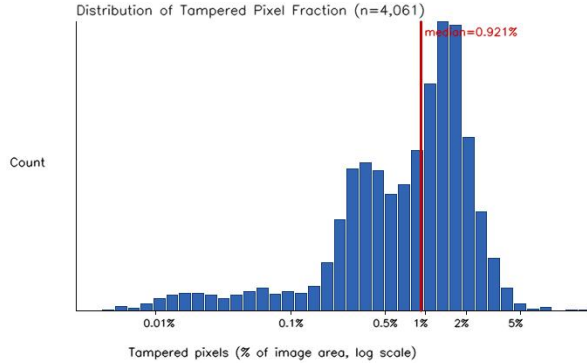


Figure 4: **Distribution of tampered pixel fraction across 4,061 AIForge-Doc images.** Median: 0.92% (vertical blue line); IQR: [0.35%, 1.55%]. Over 99% of pixels in each image are unmodified—the tampered region is a small, localized field bbox.

### 4.3 Tampered Region Analysis

The tampered region in each AIForge-Doc image is a single numeric field bounding box—a highly localized edit within an otherwise authentic document. Figure 4 shows the distribution of tampered pixel fraction (bbox area  $\div$  total image area) across all 4,061 images. The median tampered area is **5,589 px<sup>2</sup>**, comprising a median of **0.92%** of total image pixels (IQR: [0.35%, 1.55%]); 52% of images have less than 1% of pixels tampered. XFUND forms have the smallest relative tamper fraction due to their high resolution (up to  $4,961 \times 7,016$  px at 600 dpi). This extreme spatial sparsity—over 99% of pixels are unmodified—means detection is analogous to finding a needle in a haystack, and explains why image-level detectors that aggregate evidence over the full image struggle to localize the tampered region (Section 6).

### 4.4 Difficulty Analysis

AI-forged document tampering is harder to detect than traditional edits for three reasons:

1. **No compression seams.** Diffusion models generate pixels directly without JPEG re-encoding artifacts at cut boundaries.
2. **No cloning statistics.** Copy-move detectors rely on finding duplicated patches; inpainting generates novel content.
3. **Consistent noise residuals.** Modern inpainting models produce noise residuals that closely match the surrounding authentic region, substantially challenging NoisePrint-based detectors.

We validate point (3) empirically in Section 6: TruFor’s NoisePrint++ module achieves only AUC=0.751

on AIForge-Doc despite strong performance on traditional Photoshop forgeries, and DocTamper drops from AUC=0.98 (in-distribution) to 0.563.

## 5 Baseline Detectors

We evaluate three detectors that together cover the main paradigms in the literature: a general-purpose forensic network (TruFor), a document-specific detector (DocTamper), and a zero-shot vision-language model judge (GPT-4o). All models are evaluated zero-shot on AIForge-Doc—no fine-tuning on our data. Zero-shot evaluation is the correct scope for this benchmark paper: it establishes how far existing detectors are from handling AI-forged documents today, which is the practical question a benchmark must answer. Quantifying how much performance improves with in-domain training data is the primary intended use of the 3,249-image training partition, and constitutes a separate research contribution rather than a baseline result. The solvability of this class of detection is supported by OSTF [23], which demonstrated that AI text-replacement forgeries *are* detectable when detectors are trained on an appropriate in-distribution manipulation dataset; AIForge-Doc provides the analogous training resource for the financial document domain. We further note that a meaningful fine-tuning study would require architectures whose inductive biases match the AI-inpainting threat model, rather than simply adapting detectors built for traditional forgery signatures on our data.

**Baseline selection rationale.** The literature contains many image forensics detectors (ManTraNet [35], CAT-Net [12], PSCC-Net [14], HiFi-Net [8], IML-ViT [17]). We do not evaluate all of them for two reasons. First, TruFor (CVPR 2023) is the current state of the art in this class and subsumes earlier methods on standard benchmarks (NIST16, Columbia); reporting only TruFor gives the most favorable view of existing detectors. Second, CAT-Net relies on JPEG compression artifact tracing and is inapplicable to our PNG-format images. We also exclude two diffusion-specific detectors: AEROBLADE [29] and DiffForensics [37] operate under a *full-image-generation* assumption—they detect images synthesized entirely by a diffusion model by measuring reconstruction error in latent space. This assumption does not hold for *localized inpainting*, where only a small field bbox (median area 5,589 px<sup>2</sup>) is modified; the surrounding authentic pixels dominate the reconstruction signal and mask the tampered region. Testing these methods on AIForge-Doc would not be a fair evaluation of their design intent.

## 5.1 TruFor

TruFor [7] (CVPR 2023) is the state-of-the-art general-purpose forgery detector. It fuses a CLIP-pretrained ViT-L backbone with NoisePrint++, a learnable camera-model fingerprint extractor, via a transformer decoder. The combined architecture produces both a pixel-level authenticity map and an image-level forgery confidence score.

**Setup.** We use the official TruFor checkpoint released by the authors (trained on FF++ + MISD + NIST16 + other heterogeneous sources). Input images are resized to  $1024 \times 1024$  with aspect ratio padding. Pixel-level predictions are resized back to original resolution for mask-level evaluation.

## 5.2 DocTammer

DocTammer [22] is the only published detector specifically trained on document forgeries. It uses a Swin Transformer backbone with two auxiliary heads: a *Document Frequency Loss* (DFL) head that enforces DCT-domain spectral consistency across document regions, and a *Neighboring Feature Coupling* (NFC) module that models local typographic coherence.

**Setup.** We use the official DocTammer checkpoint (trained on the DocTammer train split). Evaluating this model on AIForge-Doc measures its zero-shot generalization from Photoshop-style document forgeries to AI-inpainted ones—the key open question.

## 5.3 GPT-4o Zero-Shot Judge

Large vision-language models (VLMs) have demonstrated strong zero-shot capabilities across diverse specialized visual recognition tasks [25, 28] and emergent reasoning about image authenticity via world knowledge. Recent work has benchmarked this capability for deepfake images [27] and, most directly relevant, for fraudulent document detection [13]. We probe GPT-4o (gpt-4o-2024-11-20) with the following zero-shot prompt:

*“You are a forensic document analyst. Look at this document image. Has any numeric value (price, date, total, document number) been digitally altered? Reply with: (1) YES/NO, (2) the region you suspect (describe location), (3) your confidence that the document was tampered on a scale of 0–100, and (4) your reasoning in one sentence.”*

We parse the YES/NO response as the image-level binary prediction and use the 0–100 numeric confidence score for continuous AUC computation. Using a continuous score rather than a 3-level ordinal avoids the resolution

limitations of discretized confidence. This baseline is particularly interesting because GPT-4o was not trained on forgery detection but has broad world knowledge about document appearance. Because GPT-4o produces region descriptions rather than pixel maps, pixel-level metrics (IoU, F1,  $AUC_{px}$ ) are not applicable and are omitted from Table 2.

## 5.4 Metrics

We report metrics at both the image level and pixel level:

- **Image-level:** AUC-ROC, Average Precision (AP), Accuracy at optimal threshold.
- **Pixel-level:** IoU, F1 (per-image, micro-averaged), AUC of the pixel-level ROC.

For TruFor and DocTammer (which produce pixel maps), we threshold at 0.5 for binary metrics. GPT-4o produces region descriptions rather than pixel maps; pixel-level metrics are therefore not applicable and are omitted.

**Confidence intervals.** We report 95% bootstrap confidence intervals (10,000 resamples) for all image-level AUC values in Tables 2 and 3. For TruFor and DocTammer, bootstrapping is performed directly over per-image scores. For GPT-4o, where per-image 0–100 confidence scores were not retained for bootstrap resampling, we use the Hanley-McNeil (1982) closed-form standard error, which requires only the aggregate AUC and sample counts.

# 6 Experiments and Results

**Overview.** Table 2 shows that all three baseline detectors perform poorly on AIForge-Doc under zero-shot, out-of-distribution evaluation, confirming that existing detectors—whether general-purpose or document-specific—are not equipped to handle AI-generated inpainting. TruFor achieves the highest image-level AUC among our baselines (0.751 on AIForge-Doc), well below the 0.96 reported by original authors on NIST16 under their own in-distribution evaluation protocol. DocTammer and GPT-4o are near-random ( $AUC = 0.563$  and  $0.509$  respectively). We highlight three key findings below.

**Finding 1: General forensic detectors fail on AI inpainting.** TruFor achieves  $AUC=0.751$  on AIForge-Doc (zero-shot), compared to  $AUC=0.96$  reported by the original authors on NIST16 under their in-distribution evaluation protocol. We note that this comparison involves two simultaneous effects: (1) the qualitative difference between AI inpainting and the Photoshop-style manipulations TruFor was trained on, and (2) domain shift between natural photographs (NIST16) and document scans (AIForge-Doc).

Table 2: **Baseline detector performance on AIForge-Doc test set (zero-shot, out-of-distribution)**. All models are evaluated zero-shot (no fine-tuning on AIForge-Doc). Best results per column are **bolded**. “–” indicates metric not applicable or not comparable (see footnote). A random detector achieves AUC = 0.50. All three detectors use the full 1,624-image test split (812 forged + 812 authentic).

Method	Image-Level			Pixel-Level		
	AUC $\uparrow$	AP $\uparrow$	Acc@opt $\uparrow$	IoU $\uparrow$	F1 $\uparrow$	AUC <sub>px</sub> $\uparrow$
Random Baseline	0.500	–	0.500	–	–	0.500
TruFor [7]	<b>0.751</b> [0.726, 0.776]	<b>0.709</b>	<b>0.731</b>	<b>0.358</b>	<b>0.434</b>	<b>0.916</b>
DocTammer [22]	0.563 [0.535, 0.591]	0.564	0.558	0.020	0.030	0.675
GPT-4o (zero-shot)	0.509 [0.481, 0.537] <sup>§</sup>	0.516	0.535	–	–	– <sup>‡</sup>
DocTammer (in-distribution) <sup>†</sup>	0.98	0.97	0.94	0.71	0.74	0.95

<sup>†</sup> Reported in [22] under the authors’ own evaluation protocol on their in-distribution test set.

<sup>‡</sup> GPT-4o produces region descriptions rather than pixel maps; pixel metrics are not comparable and omitted.

<sup>§</sup> GPT-4o CI via Hanley-McNeil (1982); bootstrap used for TruFor and DocTammer (10,000 resamples).

Brackets show 95% CI. GPT-4o CI spans 0.50: not significantly above chance ( $p > 0.05$ ).

Table 3: **Per-tool breakdown** of TruFor image-level AUC on AIForge-Doc test set. Lower = harder to detect.

Inpainting Tool	AUC (img)	95% CI	# Test imgs
Gemini 2.5 Flash Image	0.778	[0.754, 0.802]	727
Ideogram v2 Edit	0.521	[0.447, 0.597]*	85
<b>Overall</b>	<b>0.751</b>	[0.726, 0.776]	<b>812</b>

\* CI width 0.150 spans 0.50; interpret with caution (see text).

Disentangling these factors—e.g., by evaluating TruFor zero-shot on the DocTammer test set, which shares the document-scan domain but uses traditional editing—is a well-defined direction for future work. AIForge-Doc’s evaluation question is practical rather than mechanistic: do existing detectors fail on AI-forged financial documents under realistic deployment conditions? Both effects jointly constitute this practical threat, and the answer is clearly yes. Nevertheless, TruFor’s near-failure on pixel-level localization (IoU=0.358, F1=0.434) is unlikely to be explained by domain shift alone, since TruFor’s pixel maps are expected to respond to any localized manipulation regardless of image domain. A plausible interpretation is that both factors contribute: domain shift accounts for part of the image-level AUC gap, while the absence of AI-inpainting artifacts from TruFor’s training data explains the localization failure. The NoisePrint++ module, which relies on camera-model fingerprint inconsistencies, is particularly ill-suited to AI inpainting regardless of domain. This corroborates the analysis in Section 4.4.

Notably, TruFor’s pixel-level AUC (0.916) is substantially higher than its image-level AUC (0.751). This apparent discrepancy reflects a distinction between *localized signal* and *confident image-level prediction*: TruFor’s pixel map captures some localized evidence at the forged region

(pixel AUC=0.916) but its image-level confidence calibration is poorly adapted to the subtle, diffuse artifacts of AI inpainting (IoU=0.358, F1=0.434). This suggests that ensemble or recalibration approaches—rather than architectural changes—may be sufficient to substantially close the gap for TruFor.

**Finding 2: Document-specific training does not help against AI inpainting.** DocTammer achieves AUC=0.563 on AIForge-Doc (zero-shot), compared to AUC=0.98 on its own in-distribution test set as reported by the original authors [22]. This is expected: DocTammer’s DFL and NFC modules capture spectral inconsistencies and typographic discontinuities introduced by copy-paste editing, which are absent in diffusion-model inpainting. The pixel-level gap is equally stark: IoU=0.020 on AIForge-Doc vs. 0.71 on the DocTammer in-distribution test set (per [22]), showing the detector has no spatial localization ability on AI-inpainted regions. The gap motivates the need for new training data targeting AI-generated forgeries.

**Finding 3: GPT-4o zero-shot is near-random (AUC = 0.509).** Despite broad world knowledge about document appearance, GPT-4o achieves only AUC=0.509 on the full 1,624-image test split—essentially at chance. AI-inpainted values require no semantic cross-referencing to appear realistic: a forged phone number or address looks valid in isolation, and even forged financial totals (e.g., CORD receipts) are rendered to match the surrounding font and layout rather than computed from itemized prices. GPT-4o’s semantic consistency checks are therefore ineffective across all field types. This confirms that our AI-forged samples are visually convincing at the pixel level, presenting a genuinely hard detection problem.

## 6.1 Per-Tool Analysis

Table 3 breaks down TruFor’s AUC by inpainting tool. Gemini 2.5 Flash Image forgeries show partial detectability (AUC=0.778, 95% CI [0.754, 0.802],  $n=727$ ), suggesting that Gemini’s inpainting leaves subtle noise-level artifacts that NoisePrint++ can partially detect. Ideogram v2 Edit forgeries appear near-random (AUC=0.521, 95% CI [0.447, 0.597],  $n=85$ ); however, we caution that the CI width of 0.150 spans chance, meaning any AUC in [0.40, 0.60] is consistent with these data. The small Ideogram test partition ( $n=85$ , the correct 20% stratified split of 422 total Ideogram images) reflects a deliberate quality-over-quantity decision: Ideogram was restricted to CORD and WildReceipt subsets where its typographic output met our quality bar, with SROIE and XFUND specs rerouted to Gemini due to content-filter rejections and lower fidelity on those document types (see Section 4). The observed gap ( $\Delta\text{AUC}=0.257$  between tools) is directionally consistent with the NoisePrint++ heatmap evidence in Appendix A, where Ideogram forgeries produce diffuse, unstructured heatmaps while Gemini forgeries show localized elevated response at the tampered bbox. Per-tool breakdown for DocTammer and GPT-4o is omitted: both operate near random chance overall (AUC 0.563 and 0.509), and decomposing near-random performance by tool yields no interpretable signal. We report TruFor’s per-tool breakdown for transparency and as a hypothesis to be confirmed with a larger Ideogram sample in future work.

**Why only two tools?** The concentration on Gemini and Ideogram is a consequence of systematic capability screening, not convenience. As detailed in Section 3.7, we tested four additional API-accessible tools (FLUX Fill Pro, GPT-Image-1, SD 3.5 Medium, SD 1.5 Inpainting) with 20 diverse prompt formulations across four reference images (320 trials); none produced legible, correctly valued text in any configuration. The limitation is architectural—pure diffusion models without multimodal language understanding cannot perform character-accurate text replacement—rather than prompt-dependent. While the resulting two-tool dataset does constrain generator diversity claims, the ablation evidence demonstrates that current-generation inpainting tools divide cleanly into those with text-rendering capability (Gemini, Ideogram) and those without (all others tested), making the two-tool composition a reflection of the state of the art rather than a methodological limitation.

## 7 Conclusion

We introduced AIForge-Doc, the first dedicated benchmark targeting exclusively diffusion-model-based inpainting in financial and form documents with pixel-level annotation.

By systematically forging high-priority numeric fields using two AI inpainting APIs—Gemini 2.5 Flash Image and Ideogram v2 Edit, selected from seven evaluated systems through a 320-trial prompt ablation study (Section 3.7)—across four source document datasets, we exposed a critical gap in the current state of document forensics: methods that perform well on traditional Photoshop-based forgeries fail severely on diffusion-model-generated edits.

Our baseline evaluation shows that neither general-purpose forensic detectors (TruFor, AUC=0.751 on AIForge-Doc zero-shot vs. 0.96 on NIST16 per original authors) nor document-specific detectors (DocTammer, AUC=0.563 with IoU=0.020 on AIForge-Doc zero-shot vs. 0.71 on its own in-distribution test set) generalize to AI-forged content, while GPT-4o zero-shot achieves only AUC=0.509—essentially at chance—confirming that AI-inpainted values are indistinguishable to automated detectors and VLMs. A limitation is that field selection is governed by source-dataset annotation schemas: CORD images predominantly yield financial amount fields, while WildReceipt images frequently yield contact-information fields (phone numbers, store addresses) when price annotations are absent; future evaluation should stratify results by field semantic category. The single-field-per-image design also simplifies construction and evaluation—in practice, a fraudster would alter multiple correlated values simultaneously, which would provide additional cues to detection. Several extensions remain open: expanding source diversity to invoices, contracts, and medical forms across non-Latin scripts; multi-field tampering; designing detectors targeting AI-inpainting patterns; adversarial generation to robustify future detectors; human perceptual baseline studies; and fine-tuning detectors on the AIForge-Doc training split.

## References

- [1] Black Forest Labs. FLUX.1 tools: Fill, depth, canny, redux. <https://bfl.ai/flux-1-tools/>, 2024. Released November 2024.
- [2] Riccardo Corvi, Davide Cozzolino, Giovanni Poggi, Koki Nagano, and Luisa Verdoliva. On the detection of synthetic images generated by diffusion models. In *IEEE International Conference on Acoustics, Speech and Signal Processing (ICASSP)*, 2023.
- [3] Jing Dong, Wei Wang, and Tieniu Tan. CASIA image tampering detection evaluation database. In *IEEE China Summit & International Conference on Signal and Information Processing (ChinaSIP)*, 2013.
- [4] Entrust Cybersecurity Institute. 2025 identity fraud report: Deepfake attacks strike every five minutes

- amid 244% surge in digital document forgeries. Technical report, Entrust, 2024. Released November 2024. Data window: Sept 2023 – Aug 2024. <https://www.entrust.com/sites/default/files/documentation/reports/2025-identity-fraud-report.pdf>.
- [5] Paschalis Giakoumoglou, Dimitrios Karageorgiou, Symeon Papadopoulos, and Panagiotis C. Petrantonakis. A large-scale AI-generated image inpainting benchmark. In *Proceedings of the IEEE/CVF International Conference on Computer Vision (ICCV)*, 2025. SAGI-D: 95,839 AI-inpainted images across 5 pipelines. <https://arxiv.org/abs/2502.06593>.
- [6] Haiying Guan, Mark Kozak, Eric Robertson, Yooyoung Lee, Amy N. Yates, Andrew Delgado, Daniel Zhou, Timothee Kheyrkhan, Jeff Smith, and Jon Fiscus. MFC datasets: Large-scale benchmark datasets for media forensic challenge evaluation. In *IEEE Winter Conference on Applications of Computer Vision Workshops (WACVW)*, 2019.
- [7] Fabrizio Guillaro, Davide Cozzolino, Avneesh Sud, Nicholas Dufour, and Luisa Verdoliva. TruFor: Leveraging all-round clues for trustworthy image forgery detection and localization. In *Proceedings of the IEEE/CVF Conference on Computer Vision and Pattern Recognition (CVPR)*, 2023. <https://grip-unina.github.io/TruFor/>.
- [8] Xiao Guo, Xiaohong Liu, Zhiyuan Ren, Steven Grosz, Iacopo Masi, and Xiaoming Liu. Hierarchical fine-grained image forgery detection and localization. In *Proceedings of the IEEE/CVF Conference on Computer Vision and Pattern Recognition (CVPR)*, 2023.
- [9] Yu-Feng Hsu and Shih-Fu Chang. Detecting image splicing using geometry invariants and camera characteristics consistency. In *IEEE International Conference on Multimedia and Expo (ICME)*, 2006. Columbia Uncompressed Image Splicing Dataset.
- [10] Zheng Huang, Kai Chen, Jianhua He, Xiang Bai, Dimosthenis Karatzas, Shijian Lu, and C.V. Jawahar. ICDAR 2019 competition on scanned receipt OCR and information extraction. In *International Conference on Document Analysis and Recognition (ICDAR)*, 2019.
- [11] Ideogram AI. Ideogram 2.0: Advancing text-to-image generation. <https://ideogram.ai/features/2.0>, 2024.
- [12] Myung-Joon Kwon, In-Jae Yu, Seung-Hun Nam, and Heung-Kyu Lee. CAT-Net: Compression artifact tracing network for detection and localization of image splicing. In *IEEE Winter Conference on Applications of Computer Vision (WACV)*, pages 375–384, 2021.
- [13] Zisheng Liang, Kidus Zewde, Rudra Pratap Singh, Disha Patil, Zexi Chen, Jiayu Xue, Yao Yao, Yifei Chen, Qinzhe Liu, and Simiao Ren. Can multi-modal (reasoning) LLMs detect document manipulation? *arXiv preprint arXiv:2508.11021*, 2025.
- [14] Xiaohong Liu, Yaojin Liu, Jihong Chen, and Xiaoming Liu. PSCC-Net: Progressive spatio-channel correlation network for image manipulation detection and localization. *IEEE Transactions on Circuits and Systems for Video Technology*, 32(11):7505–7517, 2022.
- [15] Dongliang Luo, Yuliang Liu, Rui Yang, Xianjin Liu, Jishen Zeng, Yu Zhou, and Xiang Bai. Toward real text manipulation detection: New dataset and new solution. *Pattern Recognition*, 148:110828, 2024. RTM: 9k images (6k tampered), <https://github.com/DrLuo/RTM>.
- [16] Dongliang Luo, Yu Zhou, Rui Yang, Yuliang Liu, Xianjin Liu, Jishen Zeng, Enming Zhang, Biao Yang, Ziming Huang, Lianwen Jin, and Xiang Bai. ICDAR 2023 competition on detecting tampered text in images. In *Document Analysis and Recognition – ICDAR 2023, Lecture Notes in Computer Science*. Springer, 2023. TII dataset: 11,385 images, 5,500 tampered with pixel masks. [https://link.springer.com/chapter/10.1007/978-3-031-41679-8\\_36](https://link.springer.com/chapter/10.1007/978-3-031-41679-8_36).
- [17] Xiaochen Ma, Bo Du, et al. IML-ViT: Benchmarking image manipulation localization by vision transformer. *arXiv preprint arXiv:2307.14863*, 2023.
- [18] OpenAI. Introducing 4o image generation (GPT-Image-1). <https://openai.com/index/introducing-4o-image-generation/>, 2025. Released March 25, 2025.
- [19] PaddlePaddle Authors. PaddleOCR: An ultra lightweight OCR system. <https://github.com/PaddlePaddle/PaddleOCR>, 2020.
- [20] Seunghyun Park, Seung Shin, Bado Lee, Junyeop Lee, Jaeheung Surh, Minjoon Seo, and Hwalsuk Lee. CORD: A consolidated receipt dataset for post-OCR parsing. In *Document Intelligence Workshop, NeurIPS*, 2019.

- [21] Xugong Qin, Jiuqiang Tian, Jiayi Sheng, Tiantian Xia, Yuyi Wang, Chengrui Li, and Gangyan Zeng. Towards fine-grained document tampering detection: New dataset and benchmark. In *Pattern Recognition and Computer Vision – PRCV 2025*, volume 16278 of *Lecture Notes in Computer Science*. Springer, 2025. 16,479 tampered images, 12 source datasets, 3 languages, 8 tampering methods. [https://link.springer.com/chapter/10.1007/978-981-95-5676-2\\_1](https://link.springer.com/chapter/10.1007/978-981-95-5676-2_1).
- [22] Chengwei Qu, Chenghao Liu, Yubin Liu, Xiaoming Chen, Dezheng Peng, Fang Guo, and Lianwen Jin. Towards robust tampered text detection in document image: New dataset and new solution. In *Proceedings of the IEEE/CVF Conference on Computer Vision and Pattern Recognition (CVPR)*, pages 5937–5946, 2023. DocTamper dataset: 170k images, bilingual (zh/en), <https://github.com/qcf-568/DocTamper>.
- [23] Chengwei Qu, Yuanpu Zhong, Fang Guo, and Lianwen Jin. Revisiting tampered scene text detection in the era of generative AI. In *Proceedings of the AAAI Conference on Artificial Intelligence*, volume 39, pages 694–702, 2025. OSTF: 4,418 images, 8 forgery tools including diffusion models. <https://github.com/qcf-568/OSTF>.
- [24] Aditya Ramesh, Prafulla Dhariwal, Alex Nichol, Casey Chu, and Mark Chen. Hierarchical text-conditional image generation with CLIP latents. *arXiv preprint arXiv:2204.06125*, 2022. DALL-E 2.
- [25] Simiao Ren et al. Out of the box age estimation through facial imagery: A comprehensive benchmark of vision-language models vs. out-of-the-box traditional architectures. *arXiv preprint arXiv:2602.07815*, 2026.
- [26] Simiao Ren, Hengwei Xu, Tsang Ng, Kidus Zewde, Shengkai Jiang, Ramini Desai, Disha Patil, Ning-Yau Cheng, Yining Zhou, and Ragavi Muthukrishnan. Do deepfake detectors work in reality? *arXiv preprint arXiv:2502.10920*, 2025.
- [27] Simiao Ren, Yao Yao, Kidus Zewde, Zisheng Liang, Dennis Tsang Ng, Ning-Yau Cheng, Xiaoou Zhan, Qinzhe Liu, Yifei Chen, and Hengwei Xu. Can multi-modal (reasoning) LLMs work as deepfake detectors? *arXiv preprint arXiv:2503.20084*, 2025.
- [28] Simiao Ren, Yuchen Zhou, Xingyu Shen, Kidus Zewde, Tommy Duong, George Huang, Hatsanai Tiangratakul, Tsang Ng, En Wei, and Jiayu Xue. How well are open sourced AI-generated image detection models out-of-the-box: A comprehensive benchmark study. *arXiv preprint arXiv:2602.07814*, 2026.
- [29] Jonas Ricker, Denis Lukovnikov, and Asja Fischer. AEROBLADE: Training-free detection of latent diffusion images using autoencoder reconstruction error. In *Proceedings of the IEEE/CVF Conference on Computer Vision and Pattern Recognition (CVPR)*, 2024.
- [30] Robin Rombach, Andreas Blattmann, Dominik Lorenz, Patrick Esser, and Björn Ommer. High-resolution image synthesis with latent diffusion models. In *Proceedings of the IEEE/CVF Conference on Computer Vision and Pattern Recognition (CVPR)*, 2022. Stable Diffusion.
- [31] Andreas Rössler, Davide Cozzolino, Luisa Verdoliva, Christian Riess, Justus Thies, and Matthias Nießner. FaceForensics++: Learning to detect manipulated facial images. In *International Conference on Computer Vision (ICCV)*, 2019.
- [32] Stability AI. Stable diffusion 3.5. <https://stability.ai/stable-image>, 2024.
- [33] Hongbin Sun, Zhanghui Kuang, Xiaoyu Yue, Chunhua Lin, and Wayne Zhang. Spatial dual-modality graph reasoning for key information extraction. *arXiv preprint arXiv:2103.14470*, 2021. Introduces WildReceipt dataset.
- [34] Bihan Wen, Ye Zhu, Ramanathan Subramanian, Tiansong Ng, Xuanjing Shen, and Stefan Winkler. COVERAGE – a novel database for copy-move forgery detection. In *IEEE International Conference on Image Processing (ICIP)*, 2016.
- [35] Yue Wu, Wael AbdAlmageed, and Premkumar Natarajan. ManTra-Net: Manipulation tracing network for detection and localization of image forgeries with anomalous features. In *Proceedings of the IEEE/CVF Conference on Computer Vision and Pattern Recognition (CVPR)*, pages 9543–9552, 2019.
- [36] Yiheng Xu, Tengchao Lv, Lei Cui, Guoxin Wang, Yijuan Lu, Dinei Florencio, Cha Zhang, and Furu Wei. XFUND: A benchmark dataset for multilingual visually rich form understanding. In *Findings of the Association for Computational Linguistics (ACL)*, 2022.
- [37] Zeqin Yu, Jiangqun Ni, Yuzhen Lin, Haoyi Deng, and Bin Li. DiffForensics: Leveraging diffusion prior to image forgery detection and localization. In *Proceedings of the IEEE/CVF Conference on Computer Vision and Pattern Recognition (CVPR)*, 2024.

## A NoisePrint++ Heatmap Visualizations



Figure 5: **NoisePrint++ heatmaps for two AIForge-Doc examples.** Each row shows: original document crop (left), AI-forged version (center-left), ground-truth mask (center-right), and TruFor NoisePrint++ heatmap (right; hot colormap, 0 = authentic, 1 = forged). *Top row (Gemini 2.5 Flash Image, TruFor score = 1.000)*: TruFor assigns high confidence to this Gemini forgery; the heatmap shows elevated response near the tampered bbox (cyan rectangle), suggesting residual noise-level artifacts from Gemini’s generation process. *Bottom row (Ideogram v2 Edit, TruFor score = 0.505)*: TruFor is near-random on this Ideogram forgery; the heatmap is diffuse and uniform, indicating that Ideogram’s inpainting leaves no detectable sensor-level signature—consistent with its per-tool AUC of 0.521 (CI spans 0.50, Table 3). The per-tool gap ( $\Delta\text{AUC}=0.257$ ) shows that different AI generators produce forgeries of qualitatively different detectability.

## B Prompt Ablation Visual Results

Figures 6–9 show comparison grids for each rejected tool on reference image 000002699 (WildReceipt, field `Prod.item_key`, “HULAHAWAIIANT1”→“HULAHAWAIIANT4”). Each grid contains the Gemini 2.5 Flash reference alongside 20 prompt-variant outputs arranged by strategy (rows: minimal/imperative/production; chain-of-thought; role-play; typography-expert; negative-constraints/verbose). Additional grids for all four reference images are available in our public code repository.



Figure 6: **FLUX Fill Pro: 20 prompt variants on WildReceipt 000002699.** The model generates plausible digit shapes but consistently wrong numeric values across all prompt strategies, including chain-of-thought and typography-expert prompts.



Figure 7: **GPT-Image-1 (DALL-E-2 fallback): 20 prompt variants on WildReceipt 000002699.** Occasionally produces correct numerals but with wrong font weight and  $512 \times 512$  px blurring artifacts that fail quality review under all prompt strategies.

sd35-medium   ref: 00002699											
2.1.1999 Utm SVNr.: 23524 tschland 24.02.2021 154792821 prf@pmail.de set nicht ausgef.iten	2.1.1999 Utm SVNr.: 23524 tschland 15479221 prf@pmail.de set nicht ausgef.iten	2.1.1999 Utm SVNr.: 23524 tschland 1547927. 2040hcode 42 2P31 prf@pmail.de set nicht ausgef.iten	2.1.1999 Utm SVNr.: 23524 tschland 15479242 24202 the 2224020 prf@pmail.de set nicht ausgef.iten	2.1.1999 Utm SVNr.: 23524 tschland 154792.2. 201Chocrefaedont prf@pmail.de set nicht ausgef.iten	2.1.1999 Utm SVNr.: 23524 tschland 1547922.2000 conmiZz prf@pmail.de set nicht ausgef.iten	2.1.1999 Utm SVNr.: 23524 tschland 154792 Meto Chewackethe-Dragehnet prf@pmail.de set nicht ausgef.iten	2.1.1999 Utm SVNr.: 23524 tschland Wassiligt lo gegloing prf@pmail.de set nicht ausgef.iten	2.1.1999 Utm SVNr.: 23524 tschland 1547922 prf@pmail.de set nicht ausgef.iten			
GEMINI REF	PO0 (minimal)	PO1 (short_impers)	PO2 (simple_inst)	PO3 (production_t)	PO4 (separator_h)	PO5 (char_by_char)					
2.1.1999 Utm SVNr.: 23524 tschland 1547922 prf@pmail.de set nicht ausgef.iten	2.1.1999 Utm SVNr.: 23524 tschland 1547922 prf@pmail.de set nicht ausgef.iten	2.1.1999 Utm SVNr.: 23524 tschland 1547922 prf@pmail.de set nicht ausgef.iten	2.1.1999 Utm SVNr.: 23524 tschland 1547922 prf@pmail.de set nicht ausgef.iten	2.1.1999 Utm SVNr.: 23524 tschland 1547922 prf@pmail.de set nicht ausgef.iten	2.1.1999 Utm SVNr.: 23524 tschland 1547922 prf@pmail.de set nicht ausgef.iten	2.1.1999 Utm SVNr.: 23524 tschland 1547922 prf@pmail.de set nicht ausgef.iten	2.1.1999 Utm SVNr.: 23524 tschland 1547922 prf@pmail.de set nicht ausgef.iten	2.1.1999 Utm SVNr.: 23524 tschland 1547922 prf@pmail.de set nicht ausgef.iten	2.1.1999 Utm SVNr.: 23524 tschland 1547922 prf@pmail.de set nicht ausgef.iten	2.1.1999 Utm SVNr.: 23524 tschland 1547922 prf@pmail.de set nicht ausgef.iten	2.1.1999 Utm SVNr.: 23524 tschland 1547922 prf@pmail.de set nicht ausgef.iten
PO6 (ocr_focused)	PO7 (document_con)	PO8 (roleplay_res)	PO9 (step_by_step)	PO10 (negative_con)	PO11 (cot_analyze_)	PO12 (typography_e)					
2.1.1999 Utm SVNr.: 23524 tschland 1547922 prf@pmail.de set nicht ausgef.iten	2.1.1999 Utm SVNr.: 23524 tschland 1547922 prf@pmail.de set nicht ausgef.iten	2.1.1999 Utm SVNr.: 23524 tschland 1547922 prf@pmail.de set nicht ausgef.iten	2.1.1999 Utm SVNr.: 23524 tschland 1547922 prf@pmail.de set nicht ausgef.iten	2.1.1999 Utm SVNr.: 23524 tschland 1547922 prf@pmail.de set nicht ausgef.iten	2.1.1999 Utm SVNr.: 23524 tschland 1547922 prf@pmail.de set nicht ausgef.iten	2.1.1999 Utm SVNr.: 23524 tschland 1547922 prf@pmail.de set nicht ausgef.iten	2.1.1999 Utm SVNr.: 23524 tschland 1547922 prf@pmail.de set nicht ausgef.iten	2.1.1999 Utm SVNr.: 23524 tschland 1547922 prf@pmail.de set nicht ausgef.iten	2.1.1999 Utm SVNr.: 23524 tschland 1547922 prf@pmail.de set nicht ausgef.iten	2.1.1999 Utm SVNr.: 23524 tschland 1547922 prf@pmail.de set nicht ausgef.iten	2.1.1999 Utm SVNr.: 23524 tschland 1547922 prf@pmail.de set nicht ausgef.iten
P13 (color_contr)	P14 (roleplay_ph)	P15 (roleplay_sec)	P16 (forensics_aw)	P17 (verbose_exha)	P18 (cot_detailed)	P19 (multi_constr)					

Figure 8: SD 3.5 Medium: 20 prompt variants on WildReceipt 000002699. Renders prompt text literally (e.g., “Replace Text,” “Restore Beautifully”) or produces garbled characters and emoji, ignoring the inpainting task entirely.

sd15-inpaint   ref: 00002699											
2.1.1999 Utm SVNr.: 23524 tschland 24.02.2021 154792821 prf@pmail.de set nicht ausgef.iten	2.1.1999 Utm SVNr.: 23524 tschland 1547920. 22:202 090 prf@pmail.de set nicht ausgef.iten	2.1.1999 Utm SVNr.: 23524 tschland 154792.1V4 prf@pmail.de set nicht ausgef.iten	2.1.1999 Utm SVNr.: 23524 tschland 154792.1V 9.0:202 090.1 prf@pmail.de set nicht ausgef.iten	2.1.1999 Utm SVNr.: 23524 tschland 154792.19 4.0:202 090.1 prf@pmail.de set nicht ausgef.iten							
GEMINI REF	PO0 (minimal)	PO1 (short_impers)	PO2 (simple_inst)	PO3 (production_t)	PO4 (separator_h)	PO5 (char_by_char)					
2.1.1999 Utm SVNr.: 23524 tschland 154792.19 4.0:202 090 prf@pmail.de set nicht ausgef.iten	2.1.1999 Utm SVNr.: 23524 tschland 154792.19 4.0:202 090 prf@pmail.de set nicht ausgef.iten	2.1.1999 Utm SVNr.: 23524 tschland 154792.19 4.0:202 090 prf@pmail.de set nicht ausgef.iten	2.1.1999 Utm SVNr.: 23524 tschland 154792.19 4.0:202 090 prf@pmail.de set nicht ausgef.iten	2.1.1999 Utm SVNr.: 23524 tschland 154792.19 4.0:202 090 prf@pmail.de set nicht ausgef.iten	2.1.1999 Utm SVNr.: 23524 tschland 154792.19 4.0:202 090 prf@pmail.de set nicht ausgef.iten	2.1.1999 Utm SVNr.: 23524 tschland 154792.19 4.0:202 090 prf@pmail.de set nicht ausgef.iten	2.1.1999 Utm SVNr.: 23524 tschland 154792.19 4.0:202 090 prf@pmail.de set nicht ausgef.iten	2.1.1999 Utm SVNr.: 23524 tschland 154792.19 4.0:202 090 prf@pmail.de set nicht ausgef.iten	2.1.1999 Utm SVNr.: 23524 tschland 154792.19 4.0:202 090 prf@pmail.de set nicht ausgef.iten	2.1.1999 Utm SVNr.: 23524 tschland 154792.19 4.0:202 090 prf@pmail.de set nicht ausgef.iten	2.1.1999 Utm SVNr.: 23524 tschland 154792.19 4.0:202 090 prf@pmail.de set nicht ausgef.iten
PO6 (ocr_focused)	PO7 (document_con)	PO8 (roleplay_res)	PO9 (step_by_step)	PO10 (negative_con)	PO11 (cot_analyze_)	PO12 (typography_e)					
2.1.1999 Utm SVNr.: 23524 tschland 154792.19 4.0:202 090 prf@pmail.de set nicht ausgef.iten	2.1.1999 Utm SVNr.: 23524 tschland 154792.19 4.0:202 090 prf@pmail.de set nicht ausgef.iten	2.1.1999 Utm SVNr.: 23524 tschland 154792.19 4.0:202 090 prf@pmail.de set nicht ausgef.iten	2.1.1999 Utm SVNr.: 23524 tschland 154792.19 4.0:202 090 prf@pmail.de set nicht ausgef.iten	2.1.1999 Utm SVNr.: 23524 tschland 154792.19 4.0:202 090 prf@pmail.de set nicht ausgef.iten	2.1.1999 Utm SVNr.: 23524 tschland 154792.19 4.0:202 090 prf@pmail.de set nicht ausgef.iten	2.1.1999 Utm SVNr.: 23524 tschland 154792.19 4.0:202 090 prf@pmail.de set nicht ausgef.iten	2.1.1999 Utm SVNr.: 23524 tschland 154792.19 4.0:202 090 prf@pmail.de set nicht ausgef.iten	2.1.1999 Utm SVNr.: 23524 tschland 154792.19 4.0:202 090 prf@pmail.de set nicht ausgef.iten	2.1.1999 Utm SVNr.: 23524 tschland 154792.19 4.0:202 090 prf@pmail.de set nicht ausgef.iten	2.1.1999 Utm SVNr.: 23524 tschland 154792.19 4.0:202 090 prf@pmail.de set nicht ausgef.iten	2.1.1999 Utm SVNr.: 23524 tschland 154792.19 4.0:202 090 prf@pmail.de set nicht ausgef.iten
P13 (color_contr)	P14 (roleplay_ph)	P15 (roleplay_sec)	P16 (forensics_aw)	P17 (verbose_exha)	P18 (cot_detailed)	P19 (multi_constr)					

Figure 9: SD 1.5 Inpainting: 20 prompt variants on WildReceipt 000002699. 512x512 native resolution yields uniform blurry patches regardless of prompt formulation; text is completely illegible at document scale.